AGU ADVANCING EARTH AND SPACE SCIENCE

Water Resources Research

RESEARCH ARTICLE
10.1029/2021WR031829

Toward a Robust, Impact-Based, Predictive Drought Metric

Sanaa Hobeichi[1,2], Gab Abramowitz[1,2], Jason P. Evans[1,2], and Anna Ukkola[1,2]

[1]Climate Change Research Centre, UNSW Sydney, Sydney, NSW, Australia, [2]ARC Centre of Excellence for Climate Extremes, UNSW Sydney, Sydney, NSW, Australia

Key Points:

- Machine learning is used to establish a relationship between droughts documented in impact reports, and a range of observed climate features
- The new drought indicator quantifies the conditional probability of drought considering climate features, and can be used for forecasting
- Random Forest trained on drought impact data allowed us to identify the full suite of circumstances that lead to impactful droughts

Supporting Information:

Supporting Information may be found in the online version of this article.

Correspondence to:

S. Hobeichi,
s.hobeichi@unsw.edu.au

Citation:

Hobeichi, S., Abramowitz, G., Evans, J. P., & Ukkola, A. (2022). Toward a robust, impact-based, predictive drought metric. *Water Resources Research*, *58*, e2021WR031829. https://doi.org/10.1029/2021WR031829

Received 15 DEC 2021
Accepted 12 JAN 2022

Author Contributions:

Conceptualization: Gab Abramowitz
Supervision: Jason P. Evans
Writing – review & editing: Gab Abramowitz, Anna Ukkola

Abstract This work presents a new approach to defining drought by establishing an empirical relationship between historical droughts (and wet spells) documented in impact reports, and a broad range of observed climate features using Random Forest (RF) models. The new drought indicator quantifies the conditional probability of drought, considering multiple drought-related climate features and their interactive effects, and can be used for forecasting with up to 3-month lead time. The approach was tested out-of-sample across several random selections of training and testing datasets, and demonstrated better predictive capabilities than commonly used drought indicators (e.g., Standardised Precipitation Index and Evaporative Demand Drought Index) in a range of performance metrics. Furthermore, it showed comparable performance to the (expert elicitation-based) US Drought Monitor (USDM), the current state-of-the-art record of historical drought in the USA. As well as providing an alternative historical drought indicator to USDM, the RF approach offers additional advantages by being automated, by providing drought information at the grid-scale, and by having forecasting capacity. While traditional drought metrics define drought as extreme anomalies in drought-related variables, the approach presented here reveals the full suite of circumstances that lead to impactful droughts. We highlight several combinations of climate features—such as precipitation, potential evapotranspiration, soil moisture and change in water storage—that led to drought events not detected by commonly used drought metrics. The new RF drought indicator combines meteorological, hydrological, agricultural, and socioeconomic drought, providing drought information for all impacted sectors. As a proof-of-concept, the RF drought indicator was trained on Texan climate data and droughts.

1. Introduction

By the mid-1980s, drought had been defined in the scientific literature in more than 150 ways (Wilhite & Glantz, 1985). Existing definitions reflect perception differences across various disciplines (e.g., meteorology, hydrology, agriculture, society and economy) of the most important impacts of droughts (Wilhite & Glantz, 1985). Research in the late 1990s grouped existing conceptual definitions into four forms of drought (AMS, 1997). Meteorological drought (also termed climatological drought) refers to a period of below normal precipitation. Agricultural or soil moisture drought is concerned with the deficiency in water available for agriculture or natural ecosystem as a result of subsequent soil moisture depletion. Hydrological drought is concerned with the direct or indirect impacts of shortfall in surface and subsurface water supply. Socioeconomic drought refers to the effect of any of the meteorological, agricultural or/and hydrological droughts on people and water-dependent economies. More recently, the IPCC report defined drought as "a period of abnormally dry weather long enough to cause a serious hydrological imbalance" (IPCC, 2014; Seneviratne et al., 2012).

Drought indicators typically assess anomalies in a particular climate feature and make drought conclusions based on pre-defined thresholds (Heim, 2002; J. Keyantash & Dracup, 2002; Yihdego et al., 2019). Among the most common indicators used in drought analysis are the Standardised Precipitation Index (SPI; McKee et al., 1993) and the Palmer Drought Severity Index (PDSI; Palmer, 1965). SPI is based solely on precipitation (P) anomaly, while PDSI simulates soil moisture anomaly from the difference of potential evapotranspiration (PET) and P. More recently (Hobbins et al., 2016), developed the Evaporative Demand Drought Index (EDDI), a drought indicator that is based solely on PET anomaly.

Drought indicators typically define a drought event as statistically anomalous in a distribution of a specific climate feature (e.g., McKee et al., 1993; Stagge et al., 2015). There are however circumstances where near-normal conditions of several climate variables occurring simultaneously lead to impactful droughts even though they wouldn't necessarily be labeled as droughts using common drought indicators. For example, in the agricultural context, moderate pre-existing soil moisture shortages combined with a moderate precipitation shortage will

likely result in a drought. None of these hydroclimatic variables, when considered in isolation, needs to be an extreme anomaly for a drought to occur (IPCC, 2014). Similarly, a pre-existing soil moisture surplus combined with abnormally low precipitation might not lead to a drought. Therefore, looking for droughts only in the extremes of a distribution can be misleading.

Furthermore, drought indicators usually focus on a narrow selection of climate or agro-hydrological variables (and sometimes a single one) and so ultimately cannot identify all forms of droughts (Van Loon & Van Lanen, 2012). Using multiple drought indicators instead of a unique indicator is also highlighted in existing studies (Xu et al., 2019). For effective drought planning and response, it is important to develop monitoring tools capable of providing drought information for all sectors impacted by droughts (Wilhite, 2009). This requires simultaneous assessment of several drought-related variables (Brown et al., 2008). Several approaches integrate various aspects of the land-atmosphere-ocean system (e.g., Azmi et al., 2016; Brown et al., 2008; Fernando et al., 2019; J. A. Keyantash & Dracup, 2004; Li et al., 2015; Xu et al., 2020; Zhang & Jia, 2013), improving drought identification. However, they were not designed to detect all forms of drought, although some exceptions exist (Azmi et al., 2016). The development of a comprehensive drought index was described by the United States Western Governors' Association (WGA) as a top priority for improving monitoring capabilities and assisting sectors at risk in planning mitigation activities (AWG, 2004).

Recent research applied machine learning techniques and other statistical methods, including regression models, data assimilation methods, and conditional probability models, to predict existing drought indices using a number of climate variables as predictor variables (Deo & Şahin, 2015; Hao et al., 2018; Khan et al., 2020; Park et al., 2016; Soh et al., 2018; Xu et al., 2018, 2020; Yang et al., 2019). These efforts enabled the reconstruction of drought indices over time and space where the original drought indices could not be developed mainly due to lack of data needed to derive them. Statistical-based drought indictors developed this way, at best, mimic the predictive capabilities of the drought indices they are trying to emulate. However, as the drought indicators are themselves not perfect, fail to accurately depict drought events. Ultimately, the enhancement brought by most of these statistical-based indicators is limited to extrapolation in time (i.e., future predictions and past reconstruction) and/or space (areas with no data)—the quality of prediction offered by the drought index did not improve (Hao et al., 2018).

Very little effort has been made to incorporate real drought impacts data in the development of drought indices (Hughes et al., 2020 is a notable exception). This is curious since, in reality, the main purpose of using drought indicators is to enable governments and water-dependent sectors to better address impacts associated with droughts (AWG, 2004). Arguably, for better decision-making in water resources and agricultural management, it is important that drought definitions only include droughts that have impacts, and avoid the very real possibility of giving false warnings about events simply because they were found in the extreme of a distribution.

The aim of this paper is to introduce a new approach to defining drought by incorporating information from previous drought events reported in drought impact reports. As far as we are aware, documented drought impact has never been directly used to improve the ability to formally identify and predict drought. In particular, the new drought indicator needs to (i) ingest a broad range of drought-related climate variables simultaneously and consider their interactive effects (ii) uncover all forms of droughts (i.e., meteorological, agricultural, hydrological and socio-economic), that lead to impacts, (iii) provide a better quantification of drought than severity categories that are based on arbitrary thresholds, (iv) not pre-define the number of droughts occurring over time.

Texas is used as the test region, taking advantage of the wealth of drought information available from drought impact reports and other resources. The following section describes the data used to train the Random Forest (RF) algorithms, and the applied methods to test and test the developed RF drought. Results are provided in Section 3, then discussed and summarized afterward.

2. Materials and Methods

A RF binary classification algorithm was trained to discern “drought” and “no drought” conditions based on monthly climate data. We developed a database that indicates, for each month during 1982–2016 and participating Texan county, whether there was a “drought” or “no drought”. We used binary labels “1” and “0” for “drought” and “no drought” respectively, and months which don't have associated drought information were

left unlabeled. We collected the data by reading through several hundred freely available reports that provide information on drought impacts and monthly weather conditions. Corresponding climate data was extracted from several global datasets of drought-related variables. Thus, the labeled data that was used to build and test the RF model comprised monthly climate data as predictor variables (or features), and two binary classes "1" and "0" as a response variable. Unlabeled data was excluded from the training and testing.

Training the RF algorithm was conducted on a random sample consisting of 75% of the labeled data, while the remaining 25% of the data was used for out-of-sample testing of the trained model. The performance of the RF algorithm was assessed across 100 different random selection of training and testing subsets and compared with commonly used drought indicators along with the US Drought Monitor (USDM), which is the state-of-the art drought monitor in Texas. A detailed description of the methodology is provided below.

2.1. Predictor Variables

Predictor variables comprise a range of drought-related climate variables and phenomena that describe the land-atmosphere-ocean system. These include monthly estimates of precipitation (*P*), surface soil moisture (SM), PET, actual evapotranspiration (ET), change in water storage (CWS), Normalised Difference Vegetation Index (NDVI), and El Niño-Southern Oscillation (ENSO). Surface soil moisture of the previous month (SM_{prev}) and the calendar month were also incorporated as predictor variables. These predictors are chosen because they are directly associated with drought development (e.g., *P*, PET, ET, SM, or interaction thereof), persistence (e.g., ET, SM, and NDVI), and/or impacts (CWS) and may have varying importance depending on a number of factors including the season (month) and the region. Incorporating ENSO as a predictor variable was guided by studies showing droughts in Texas are related to La Niña events, which affect Pacific moisture patterns (Pu et al., 2016; Schubert et al., 2004; Seager et al., 2014). SM_{prev} was used to provide information on the resilience of the system to withstand drought. Most of these predictor variables appear in existing drought monitoring approaches(Beguería et al., 2014; Brown et al., 2008; Hao et al., 2018; Karnieli et al., 2010; McKee et al., 1993; Nanzad et al., 2019; Ukkola et al., 2018).

The source and reference of each dataset are provided in Table 1. The spatial resolution of all the employed gridded datasets is 0.25° except PET and CWS which have a coarser resolution of 0.5°. All the gridded datasets are resampled to a common 0.5° grid using nearest neighborhood interpolation. Predictor variables are then extracted at 30 grid points (Figure 1) in all time steps during 1982–2016 where matching drought event labels are available. The 30 grid points are located in 30 counties, most of them are about the size of a grid cell, that is, 0.5°. These are distributed over all 12 Texan eco-regions identified by the United States Environmental Protection Agency (EPA, https://www.epa.gov/; Figure 1).

2.2. Binary Database of "Drought" and "No Drought" Events

"Drought" and "no drought" events attributed to a grid cell during a period of time are based on information extracted from two main sources. "Drought" included effective droughts, whereas "no drought" includes wet conditions and marginal water stress conditions'. The source that contributed to most of the "drought" events is the Drought Impacts Reporter (DIR), a national interactive drought impact database developed and maintained by the U.S. National Drought Mitigation Center (NDMC; Wilhite et al., 2007). Sources contributing to the DIR database include news articles, scientific publications, National Weather Service Drought Information Statements, agency reports, and reports submitted by government officials and the public. The DIR comprises information on drought impacts reported by a wide range of drought-impacted sectors. Submitted reports from any source are then reviewed for drought impact information and verified by NDMC before becoming publicly available at https://droughtreporter.unl.edu/. Reported impacts include the agricultural sector, livestock, water, energy, and fire sectors, social impacts, forestry, recreation and tourism, and more.

A major source of "no-drought" events are the Texas Climate Monthly Reports (TCMR), monthly bulletins produced by the Office of the State Climatologist at Texas A&M University. They provide a summary of weather conditions throughout Texas, describe big weather events such as floods, storms, and hurricanes, and report the number of days with rain and monthly precipitation totals picked up in several locations. Monthly bulletins are produced from 1990 onwards and can be accessed at https://climatexas.tamu.edu/products/texas-climate-bulletins/index.html.

Table 1
Climate Variables Used as Predictor Variables

Climate variable and unit × month^{-1}	Name and Reference	Temporal and spatial coverage and resolution	Data description and access link
Change in total water storage (mm)	GRACE-REC (Humphrey & Gudmundsson, 2019)	1979-2016 monthly 0.5° global land	JPL_MSWEP – 1st member: Statistical model trained with GRACE JPL mascons and forced with MSWEP precipitation. The change in total water storage in a given month was computed by subtracting the total water storage anomalies of the previous month from the current month. https://figshare.com/
Evapotranspiration (mm)	DOLCE V2.1 (Hobeichi, 2020) (Hobeichi et al., 2021)	1980-2018 monthly 0.25° global land	Observationally constrained hybrid evapotranspiration product derived by merging 11 available ET products. http://dx.doi.org/10.25914/5eab8f533aeae
Precipitation (mm)	GPCC V2018 (Schneider et al., 2018)	1891-2016 monthly 0.25° global land excluding Antarctica	Monthly Land-Surface Precipitation from Rain-Gauges built on GTS-based and Historical Data https://psl.noaa.gov/data/gridded/data.gpcc.html
Potential Evapotranspiration (mm)	Priestley-Taylor PET	1901-2017 monthly 0.5° global land excluding Antarctica	Calculated from CRU TS4.02 (Harris et al., 2014) monthly cloud cover and mean temperature using the R package *rstash* (https://github.com/rhyswhitley/r_stash; Davis et al., 2017) CRU TS4.02 data can be accessed via https://catalogue.ceda.ac.uk/uuid/b2f81914257c4188b181a4d8b0a46bff
Soil moisture of the current and previous months (m^3 m^{-3})	CCI-SM (Gruber et al., 2019) (Gruber et al., 2017) (Dorigo et al., 2017) (Liu et al., 2012)	1979-2019 daily 0.25° daily global land excluding land covered with snow	COMBINED CCI Soil Moisture product datasets v04.7 https://esa-soilmoisture-cci.org/
month		1980-2016	Calendar month
ENSO Index	(Smith & Sardeshmukh, 2000)	1870-2020 1-month running mean	A Bivariate EnSo Timeseries or the "BEST" ENSO Index it combines (i) SOI: Southern Oscillation Index (based on the observed sea level pressure differences between Tahiti and Darwin) and (ii) Niño 3.4 SST (NINO3.4 is the average sea surface temperature anomaly in the region bounded by 5°N to 5°S, from 170°W to 120°W) based on the mean climatology for the period 1871-2001. https://psl.noaa.gov/
NDVI	NASA-GIMMS v1.1 (Pinzon & Tucker, 2014)	July 1981 to Dec 2017 0.0833° bimonthly	NDVI from Advanced Very High Resolution Radiometer, averaged to monthly by taking the maximum of bimonthly values https://gimms.gsfc.nasa.gov/

Building the database of Texas drought events involved a careful assessment of the DIR, TCMR, and relevant literature. Periods where regions were trending toward drought or recovering from it are not marked as events. Furthermore, we excluded reports of small scale impacts and only included county scale impacts; this ensured scale consistency between observed drought impacts and the measured drivers described in Section 2.1.

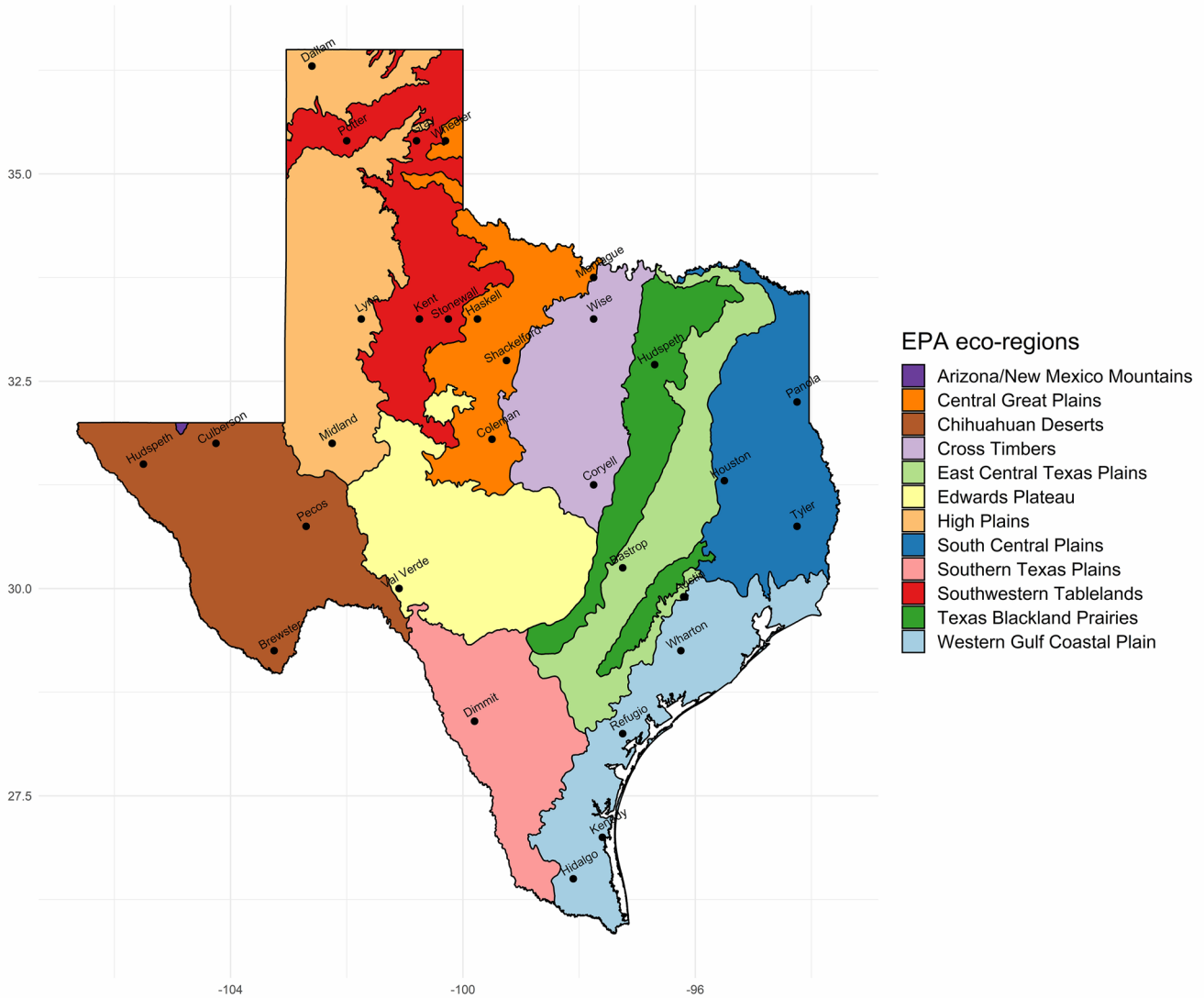

Figure 1. Location of 30 grid cells used in this study over a layer of Texas ecoregion map (level 3) developed by the EPA (https://www.epa.gov/).

The final (spatiotemporally incomplete) database for this test case comprises a total of 1005 records in 500/505 split for "no drought" and "drought" respectively. Each record consists of a location (a county), a time (year and month) and a label ("drought" or "no drought"). Table S1 in the Supporting Information S1 shows these records along with the relevant source.

2.3. Random Forest Algorithm

2.3.1. Building a Random Forest Classification and Probability Model

Random forest algorithm (Breiman, 2001) grows a collection of classification trees (or alternatively probability trees) each fitted on bootstrap samples (samples are drawn with replacement) of labeled data (predictor variables and associated labels) available for training. As a result of the bootstrapping procedure, trees in the forest are trained on different—but not mutually exclusive—subsets of labeled observations. In each tree, data undergo recursive binary splits based on the predictor variables. The sample data at a parent node is split on a predictor's cutoff value (e.g., $P = 100$ mm) and results into exactly two child nodes. A subset of predictors of predefined size is available for the split at each node. The RF algorithm carries out an optimization procedure that controls the selection of an appropriate predictor at each node, the cutoff values at which the data will split, and whether there

will be further splitting. These decisions are based on a metric known as the Gini index (Breiman et al., 1984) which measures the relevance and consequence of each feature available for split at each node, and that ensures that as the trees grow, the impurity decreases, that is, the variance within subsequent child nodes decreases. Each tree keeps growing until the impurity does not decrease further, or until the number of samples in the terminal node—also called leaf node—falls below a threshold.

Each terminal node in the forest is assigned a class "drought" or "no drought" and a probability of drought. The class represents the majority label in the terminal node. The probability of drought is equal to the proportion of "drought" labels at the terminal node, and it represents the conditional probability of drought emergence given the features described from the top of the tree down to this terminal node. The reliability of conditional probabilities computed by the RF approach is examined and demonstrated by Malley et al. (2012).

This work applies a new implementation of RF developed in the "RANdom forest GEneRator" (ranger; Wright & Ziegler, 2017), an open source software package in R. Ranger provides a higher computational speed and better memory storage efficiency compared to other available implementations [e.g., Random Jungle (Kruppa et al., 2014), and Random Forest (Liaw & Wiener, 2002)] while maintaining a similar performance (Wright & Ziegler, 2017). We used the default parameters described in the ranger package to build both the RF classification model and a RF probability model. These involve 500 trees, three predictor variables available for split at each node (i.e., mtry = $\sqrt{\text{number of features}}$), and the same size as the training dataset is used for number of bootstrap samples. It is recommended to set the number of trees to a computationally feasible large number (Hengl et al., 2018). Since the processing time was negligible (<10 milliseconds for training), we used a large number of trees, that is, 500. The selected value for the "mtry" hyperparameter (i.e., 3) was identified by a 10-fold cross validation test as the optimal mtry value.

It is important to note that the sub-sampling of predictors at each node along with the bootstrapping procedure and the fact that trees are built in parallel force variation between trees and ensure that they have a small pairwise correlation.

The outcome from training the RF algorithm on drought event data can be either a RF binary classification model or a RF probability model. This is determined during the training process and is based on whether the purpose is to classify new samples as "drought" or "no drought", or to compute the conditional probability of drought. Here we developed and used both models.

2.3.2. Prediction

To predict the binary class and the drought probability of a given new sample, its driver values are propagated through all the trees in the forest, and the terminal node values at each tree—which have been calculated during the training process for both class and the probability—are collated. The final class assigned to the new sample is based on the majority class from all trees, and the estimated conditional probability of drought is the average probability estimate over all trees.

2.3.3. Variable Importance

We use conditional permutation to assess the importance of each predictor variable as described in (Strobl et al., 2008). To measure the importance of a particular predictor variable, for example, ET, ET is randomly permuted, then predictions are made using the remaining variables and the permuted variable (substitute of ET). The difference in prediction accuracy before and after permuting ET averaged over all permutations in the forest is used as a metric of its importance. The most important variable is the one that achieves the largest reduction in prediction accuracy when randomly permuted. Conditional permutation variable importance reflects the true impact of each predictor variable more reliably than the default variable importance scheme in the Ranger package, namely Gini importance (Sandri & Zuccolotto, 2008). For each predictor variable, Gini importance measures the reduction in impurity on the response variable achieved by each predictor at every split across all nodes in all trees. The conditional permutation importance was proven more reliable than the Gini importance in situations where some predictor variables are highly pairwise correlated (Strobl et al., 2008), and/or have different scales of measurement and categories (Strobl et al., 2007). Conditional permutation variable importance was derived using the R party package (http://party.R-forge.R-project.org).

2.4. Comparison of Drought Indicators

We compared the prediction skill of the RF drought indicator (tested out-of-sample) with commonly used drought indicators. We provide a quick summary of these, and refer readers to the associated publications for further details.

SPI: Assesses drought solely from precipitation. At a given location, long term monthly precipitation is transformed into a normal distribution, and the computed SPI value represents the unit standard normal deviate. Previous studies have associated droughts with SPI values of less than −1 for example, (Bachmair et al., 2015), −0.8 (in USDM) or 0 (McKee, 1995). We calculated monthly SPI using the SPEI R package for each grid point presented in Figure 1 from the same precipitation dataset used to develop the RF model. We derived SPI for several accumulation periods including 1, 3, 6, 9 and 12 months. In this study we carry out the analysis using each of the three drought cutoffs, that is, −1, −0.8 and 0.

Evaporative Demand Drought Index (EDDI; Hobbins et al., 2016): monitors drought solely from PET anomalies, where PET is derived using the American Society of Civil Engineers standardized reference ET equation (Walter et al., 2000), which estimates PET by simplifying the Penman-Monteith equation mainly from satellite-based estimates of temperature, humidity, windspeed, and solar radiation. Unlike SPI, the probability distribution of PET is computed empirically using an inverse normal approximation. Positive (negative) EDDI values are commonly used to discern drought (no drought) conditions. We downloaded EDDI maps for the period 1980–2016 from https://psl.noaa.gov/eddi/ using the R package "eddi".

PDSI: assesses droughts using anomalies of soil moisture, where soil moisture is calculated from P and PET using a simple soil moisture balance model. Negative (positive) PDSI values are used to discern drought (wet) conditions. In this work we calculated PDSI from the same P and PET datasets used to develop the RF drought indicator. We used the R package scPDSI to calculate a self-calibrated version of PDSI.

The U. S. Drought Monitor (USDM; Svoboda et al., 2002): is currently the state-of-the-practice for drought monitoring in the U.S. It consists of weekly maps that show regions where land has been Abnormally Dry (D0), or in drought with intensity ranging from moderate (D1) to exceptional (D4). Drought categories are produced from blending i) several drought indices including SPI and PDSI, (ii) the analysis of various observed and modeled climate variables such as P, temperature, snow water equivalent, water in the soil, streams, lakes and others, (iii) reported drought impacts, and (iv) experts assessment of (i), (ii) and (iii) and judgments. In this sense USDM is a retrospective, assimilated observationally-based product, that could not, for example, be applied to climate projections. The spatial resolution of the USDM Maps is the approximate scale of a climate division, that is 10 regions in Texas. USDM maps are available from 2000. We downloaded USDM maps from https://www.drought.gov/drought/ and aggregated weekly maps into monthly binary "drought"/"no-drought" maps whenever possible. Regions consistently in drought (non-drought) during a month were labeled "drought" (no-drought), whereas regions that were in drought during part of the month were not used in the comparison.

2.5. Out-of-Sample Testing and Performance Metrics

We assessed the performance of the RF algorithm by testing its ability to correctly classify unseen events (not used in training). To achieve this, 75% of events were used to train the RF model, and the remaining 25% of events used to test it. The 75/25 sampling was randomized 100 times to create 100 different RF models. The performance of the RF approach was then assessed by comparing the performance of each RF model at its 25% of out-of-sample events, and aggregating across the 100 cases. Six statistical metrics commonly used in binary classification were then used to compare the out-of-sample success of the RF model compared to existing drought metrics:

- Accuracy: correct predictions expressed as a fraction of total predictions
- False alarm rate: incorrect "drought" predictions expressed as a fraction of all "drought" predictions
- Success ratio or precision: correct "drought" predictions expressed as a fraction of all "drought" predictions
- Threat Score or Critical Success Index: measures how well "drought" predictions correspond to "drought" observations. It is calculated as correct "drought" predictions expressed as a fraction of both "drought" predictions and "drought" observations combined

- True positive rate or sensitivity (also known as recall and hit rate): correct "drought" predictions expressed as a fraction of "drought" observations
- True negative rate of specificity: correct "no-drought" predictions expressed as a fraction of "no-drought" observations

A perfect score is 0 for the "False alarm rate", and 1 for all the other performance metrics.

We computed these performance metrics for the RF-drought indicator, EDDI, PDSI, SPI, and USDM at all 100 testing datasets. We also assessed the predictive ability of eight other well-known machine learning classifiers (Balakrishnama & Ganapathiraju, 1998; Breiman, 2001; Friedman, 1991; Kuhn, 2008; Mitchell, 1997; Nelder & Wedderburn, 1972; Scholkopf et al., 1997; Swain & Hauska, 1977; Wilhite et al., 2007; Zou & Hastie, 2005) trained with the same training datasets as the RF classifier, by computing these performance metrics across the same 100 out-of-sample testing iterations. The other machine learning algorithms are listed in Table S2 in the Supporting Information S1, we refer the reader to the associated publications for description of each algorithm.

3. Results

3.1. Performance of RF and Other ML Classifiers Out-of-Sample

Figure 2 shows the performance results of the RF and other ML classification algorithms, each trained on 75% of events and tested out-of-sample at 25%, across 100 random selections of training and testing samples. Random forest achieves above 90% score in accuracy, true positive, true negative and success ratio across the majority of iterations. The median threat score exceeds 80%, and the median false alarm rate is about 10%. In comparison with the other ML approaches, overall, the random forest algorithm performs the best across all metrics. The statistical significance of the improved scores of RF compared to the other ML algorithms is confirmed with a two-tailed *t*-test performed for each performance metric at 0.05 significance level.

The competitiveness of RF with the best available ML algorithms has been demonstrated across a range of applications (e.g., Cutler et al., 2007; Fernández-Delgado et al., 2014; McGovern et al., 2017; Park et al., 2016; Rodriguez-Galiano et al., 2012). Figure 2 shows that RF stands out as much more capable than the other employed ML algorithms in identifying teleconnections between climate features and droughts. There are two additional benefits in using RFs. First, RF is capable of quantifying the conditional probability of drought, a very important feature that is not found in most other classifiers. Also, as highlighted in Section 2.3.2, RF allows the assessment of the importance of its predictor variables, which gives insight into the factors influencing droughts, as well as the least important climate features in explaining and quantifying droughts in different circumstances.

3.2. Performance of RF Out-of-Sample, Compared to SPI, PDSI, EDDI and USDM

Figure 3 illustrates the performance results of the RF drought indicator relative to EDDI, PDSI, USDM and SPI computed for 6 months accumulation period (at two drought cutoffs, −0.8 and 0, denoted by $SPI_{-0.8}$ and SPI_0 respectively). The drought indicators are computed across the 100 different testing datasets. Overall, RF and USDM achieve the highest scores across all metrics followed by $SPI_{-0.8}$ and SPI_0. We exclude SPI at −1 drought cutoffs from the plot as it consistently shows inferior performance than each of $SPI_{-0.8}$ and $SPI_{0.}$

Figure 3 shows that the RF approach is more accurate than EDDI, SPI (at both thresholds), and PDSI, and has comparable accuracy to USDM. While the accuracy metric provides a summary of performance, the true positive and true negative scores compare the ability to correctly predict drought and no drought, respectively. USDM, EDDI, SPI_0 and PDSI appear to do significantly better in identifying "drought" compared to "no drought". This indicates that most of the inaccuracy in these three indicators come from their tendency to mistakenly predict "drought" when there is actually "no drought". The RF approach scores higher than USDM in True negative and lower in True positive. The difference in score between True positive ratio and True negative ratio is the smallest in the RF approach and the highest in EDDI. Overall, the score of the RF approach is the least variable across the six performance metrics among all the indicators. The RF approach gives fewer false alarms of droughts than the other indicators and has the best success ratio.Both USDM and RF stands out in the "threat score",with USDM scoring a slightly higher, but not statistically different mean threat score than that scored by the RF drought indicator. We compare the mean scores achieved by USDM and RF-drought indicator across all the metrics of

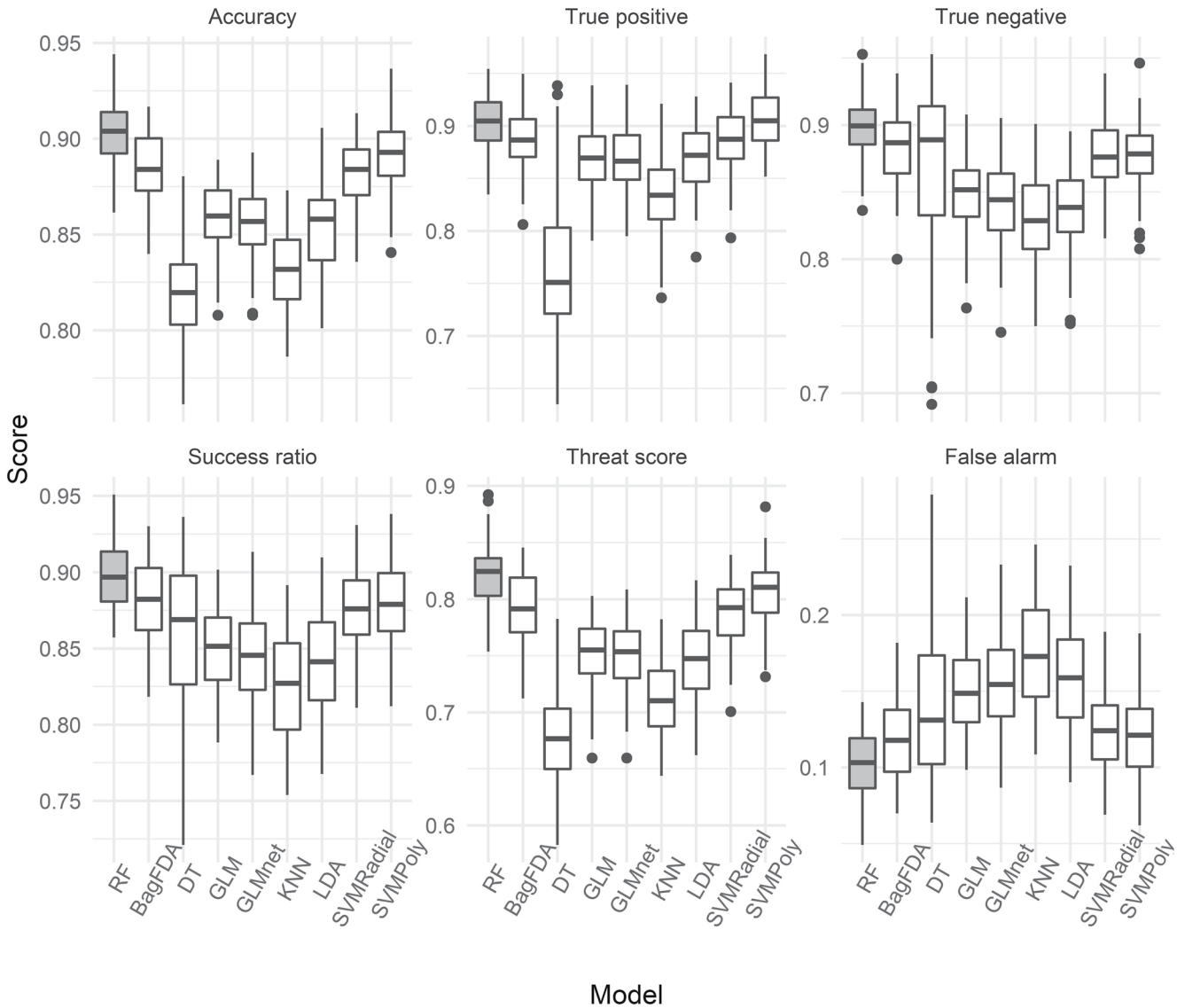

Figure 2. Performance results of RF classification algorithm and nine other ML classifiers at testing samples across 100 different sub-sampling of training and testing samples. Performance scores are explained in Section 2.5. The other ML classifers are Bagged Flexible Discriminant Analysis (BagFDA; Friedman, 1991), Decision Tree (DT; Swain & Hauska, 1977), Generalised Linear Models (GLM; Nelder & Wedderburn, 1972), Lasso and Elastic-Net Regularized Generalised Linear Models (GLMnet; Zou & Hastie, 2005), K-nearest Neighbors (KNN; Mitchell, 1997), Linear Discriminant Analysis (LDA; Balakrishnama & Ganapathiraju, 1998), Support Vector Machine radial basis kernel (SVMRadial), and Support Vector Machine polynomial basis kernel (SVM Poly Scholkopf et al., 1997). A brief description of each dataset is provided in Table S1 of the Supporting Information S1.

performance using a *t*-test, and we find that whenever the mean scores of the RF-drought indicator and USDM are statistically different at 5% significance level, the RF-drought indicator outperforms USDM (Table S3 in Supporting Information S1).

PDSI shows poor performance overall. It was previously reported that monthly PDSI do not capture droughts on short time scales, that is, less than a year (Dai, 2019). SPI computed for 6 months accumulation period performed the best compared to the other examined accumulation periods (i.e., 1, 3, 9 and 12), and its performance varies according to the drought cutoff. At a −0.8 cutoff, where droughts correspond to SPI ≤ −0.8, $SPI_{-0.8}$ scored low in True positive and threat score, which indicates that $SPI_{-0.8}$ tends to miss droughts. This explains why $SPI_{-0.8}$ achieved a near optimal score in the True negative metric. In contrast, at a 0 cutoff, SPI_0 scored low in True negative and a near optimal score in True positive, which indicates that SPI_0 tends to predicts drought when there is actually no drought.

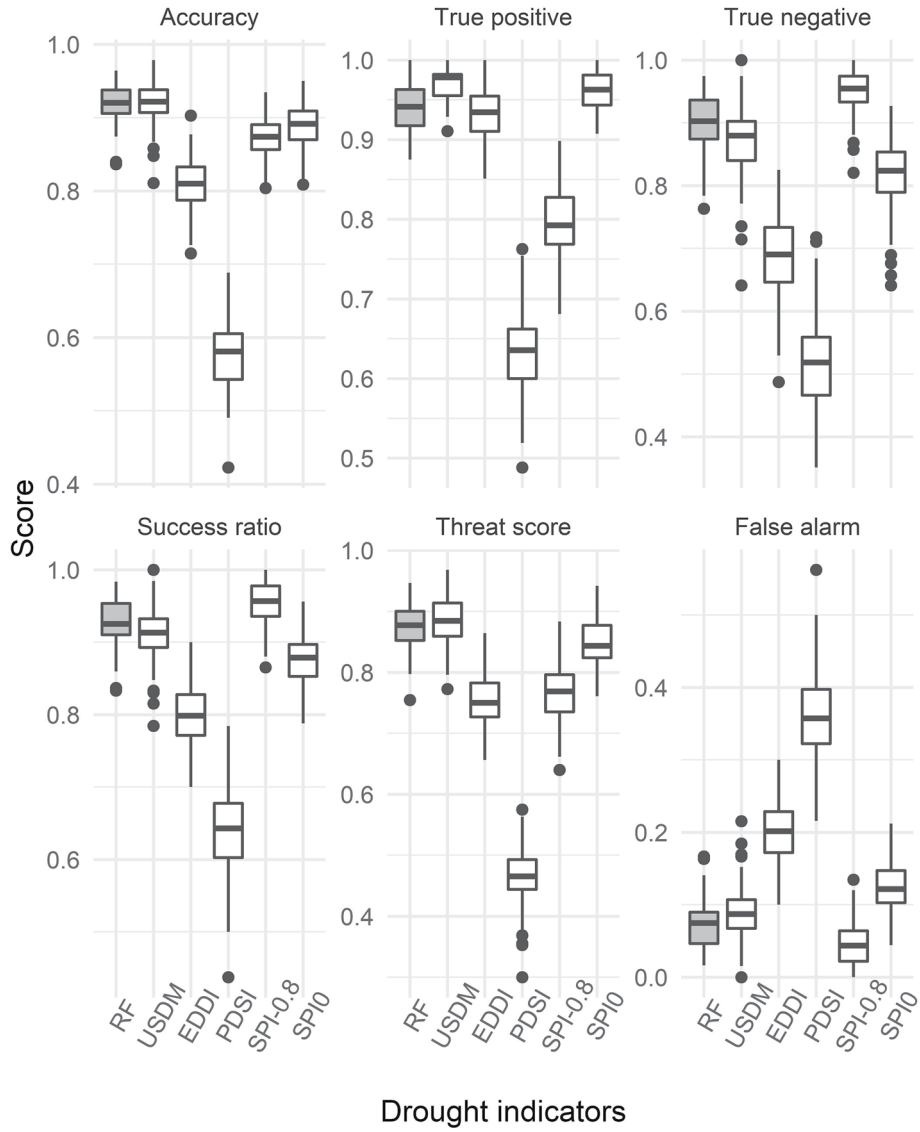

Figure 3. Performance scores of RF classifier and commonly used drought indicators, that is, USDM, EDDI with drought threshold value of 0, PDSI with drought threshold value of 0, and SPI with drought threshold values of 0 (SPI_0) and −0.8 ($SPI_{-0.8}$) and computed for a 6-month accumulation period. Scores are computed at testing samples across 100 different sub-sampling of training and testing samples. Performance scores are explained in Section 2.5.

3.3. RF Drought Probability Maps

We built the final RF drought indicator for Texas on all event data without excluding a proportion for testing. In Figures 2 and 3, the purpose of training the RF algorithm on a subset (75%) of the labeled of data was to test the RF algorithm on unseen data and get a robust estimate of the derived RF model. Here, the RF model trained on all the labeled samples is used to predict the probability of drought at every grid cell and time step based on the values of the predictors (as explained in Section 2.3). This produced drought probability maps for Texas. In the following, we reference a Texas Climate Monthly Reports (TCMR) of a given month, for example, January 2010 as TCMR/1-2010, where the actual reference is https://climatexas.tamu.edu/products/texas-climate-bulletins/january-2010.html. We reference an impact report from the DIR database as DIR followed by its impact ID, for example, DIR4115.

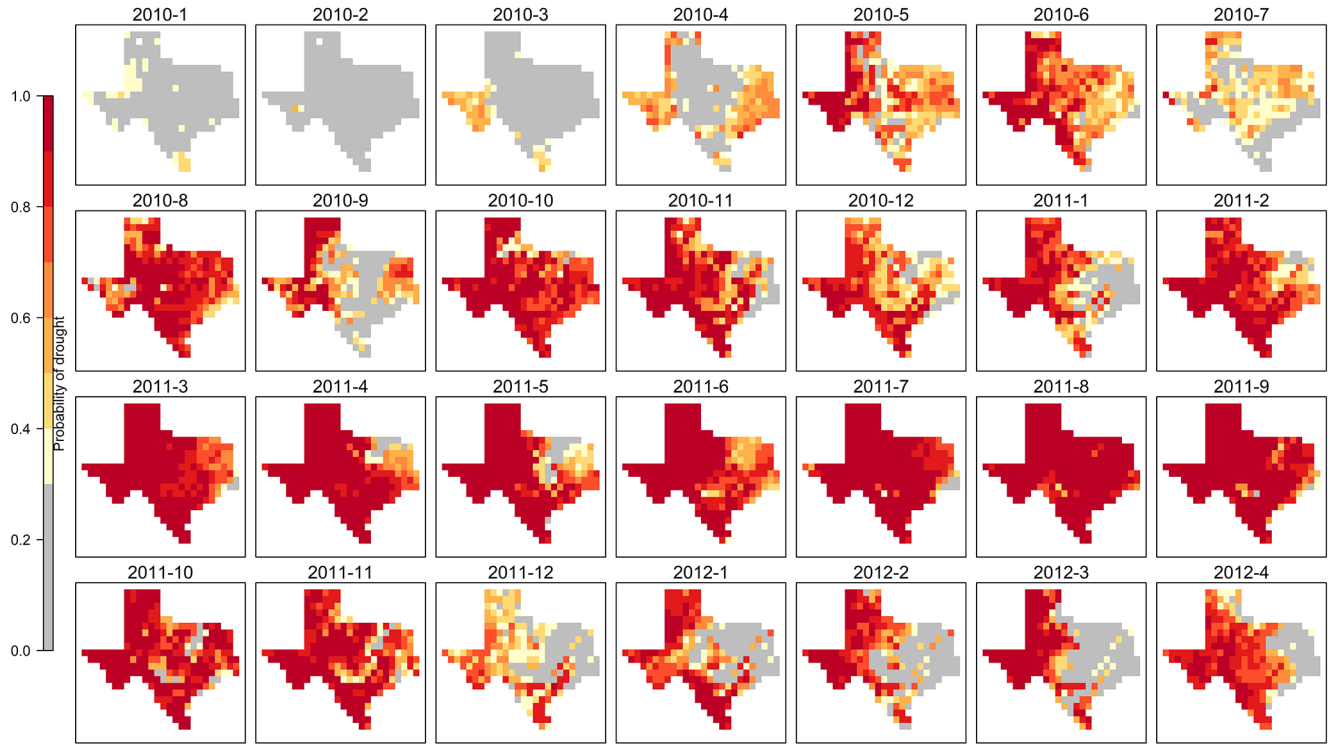

Figure 4. Drought probability maps predicted by RF during a drought episode.

3.3.1. The 2011 Drought

We examined a drought episode over Texas during 2010–2012 (known as the 2011 drought) using drought probability maps derived by the new RF drought indicator for the period spanning from January 2010 to April 2012. The 2011 drought was considered one of the most catastrophic short-term droughts in the US and caused tremendous agricultural, hydrologic, economic and socio-economic losses (Combs, 2014; Grigg, 2014). It was thought to be linked to strong La Niña conditions in the Pacific which were established in the fall of 2010 and were responsible for the below normal rain received during 2010–2012 (Folger et al., 2012; Texas Water Development Board, 2012). The drought probability maps in Figure 4 illustrate how the 2011 drought progressed in time and space throughout the examined period.

Weather stations across Texas reported abundant precipitation during winter 2010 (TCMR/1-2010, TCMR/2-2010, TCMR/3-2010, TCMR/12-2010). As soon as the spring began, dry conditions were felt statewide. According to impact reports, dry conditions were reported in the South central plains, Western Gulf Coastal Plain (DIR4115) and Panhandle from March 2010. In the next months, dry conditions worsened and caused severe impacts on the growing season (DIR25697). The drought probability maps in Figure 4 show an increase in drought probability from April through June, starting in Panhandle, west and south Texas and expanding gradually to the entire state. The first half of July brought substantial rain (TCMR/7-2010) due to Hurricane Alex, which according the probability map has temporarily obliterated drought in most of Texas. The very dry and very hot August (TCMR/7-2010) appeared to have quickly wiped out the moisture brought by the wet spell in July; this is reflected in the increase in drought probabilities. In September 2010, a tropical storm brought significant rain along the Western Gulf Coastal Plain, Southern Texas Plains and East Central Texas plain (TCMR/9-2010), which as indicated in the September 2010 map temporarily broke the drought in these regions. Rain was also picked up by areas in the west and in the Panhandle, however, due to the very high temperatures, these areas were not relieved from the drought as observed in the drought probability map of September 2010. Very dry and very warm conditions returned in October (TCMR/10-2010) and quickly elevated drought probabilities. The drought areas, and many parts of Texas did not receive a single trace of rain. By the end of fall, drought exacerbated in Bastrop (DIR14853), Austin (DIR25214), Panhandle (DIR 3667), and many areas across the state were reported as natural disaster areas (DIR4115). The eastern part of the state experienced cold weather and rainy respite in

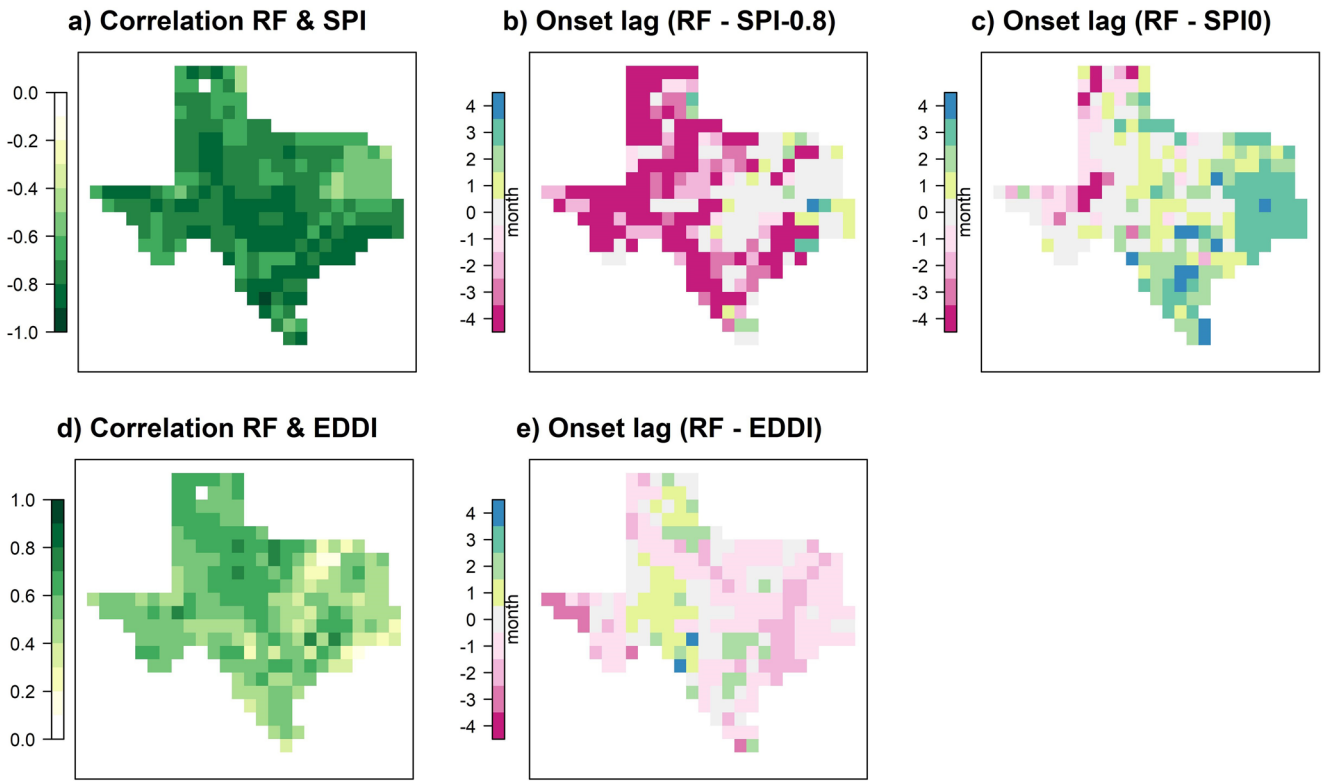

Figure 5. Correlation between RF drought probabilities and (a) SPI, and (d) EDDI. Difference in RF drought onset and each of (b) SPI with a drought threshold of −0.8 (i.e., $onset_{RF} - onset_{SPI\text{-}0.8}$), (c) SPI with a drought threshold of 0 (i.e., $onset_{RF} - onset_{SPI0}$) and (e) EDDI (i.e., $onset_{RF} - onset_{EDDI}$). Correlations and onsets are computed for the period spanning January 2010-April 2012.

January 2011 (TCMR/1-2011), which lowered the percentage of the land in drought. In February 2011, Texas experienced sub-zero temperatures with scarce precipitation (TCMR/2-2011), which put most of the state under drought. Probability maps show that drought conditions continued throughout Texas in March 2011. In April 2011, abnormally dry and warm weather continued across the entire state. According to drought reports, since the beginning of 2011, bushfires devastated thousands of acres almost everywhere (DIR4160, 4158, 4167, 3937, 4199, 4166, 4120, 4167). By April, the water level in lakes, wetlands and rivers had reached very low levels (DIR3667, 4212, 25,155), and voluntary and compulsory reduction in water use was imposed in many areas across the state (DIR 24648, 3879). In April and May, the Dallas region in northern Texas picked up drought breaking rains (TCMR/4-2011, TCMR/5-2011) which helped reduce the probability of drought before the abnormally warm summer had started (TCMR/6-2011). Drought continued during the summer causing more wildfires (DIR4465) and tremendous losses in agriculture statewide (DIR29694, 26,744, 4019, 4022, 14,864, 3965). The drought persisted the entire 2011, however there were a few cold fronts that brought important rain over many areas in the eastern part of the state (TCMR/11-2011) in November, and the relieved areas experienced temporary decrease in drought probability during that month. December 2011 was in general wetter than usual in most of the state except in the far west (TCMR/12-2011). This is reflected in the significant decrease in drought probability during this month. January 2012 was another wetter than usual month. Substantial rain was observed in all weather stations except in the Panhandle, Rio Grande Valley and most of the Far West (TCMR/1-2012). The drought probability maps for the months of January-April 2012 show a drought free area stretching from the Central Great Plains to the South Central Plains.

3.3.2. Comparing RF Drought Indicator With EDDI and SPI Indices in Representing the 2011 Drought

We assessed the agreement between the RF drought indicator and EDDI and SPI in representing the 2011 drought during January 2010 and April 2012 using two metrics: correlation and difference in drought onset. The correlation between the RF drought probabilities and SPI is very strong everywhere (Figure 5a). In fact, unsurprisingly, precipitation was found to be the most explanatory variable in discerning “drought” and “non drought”

Table 2
Importance of Hydro-Climatological Variables in Discerning "Drought" and "No Drought" Measured Using Conditional Permutation Scheme (Strobl et al., 2008)

Importance rank	1	2	3	4	5	6	7	8	9
Climate feature	P	ENSO	SM	SMprev	ET	CWS	PET	NDVI	Month
Mean	0.089	0.069	0.058	0.0165	0.0073	0.0073	0.0058	0.0038	0.0028
Range	[0.084 – 0.096]	[0.066 – 0.073]	[0.053 – 0.064]	[0.0138 – 0.019]	[0.006 – 0.0088]	[0.0057 – 0.008]	[0.0045 – 0.0072]	[0.0027– 0.0052]	[0.002 – 0.0037]

Note. "Mean" (range) is the mean (range of) importance computed across 100 generated RFs.

as described in more detail below. Negative correlations were obtained because drought is denoted by negative values in SPI and higher (positive) probabilities in RF. In comparison, the correlation between RF and EDDI in Figure 5d is high (0.5–0.8) in the western half of the state but weakens in the eastern half of the state, with the lowest correlation observed in the Cross Timbers regions.

We examined the difference in drought onset with SPI at the two drought thresholds and over several accumulation periods. Figures 5b and 5c display the results for $SPI_{-0.8}$ and SPI_0 respectively, both computed for 1-month accumulation period. Drought appears in RF drought index well in advance of $SPI_{-0.8}$ across the dry western half of the state and the majority of the state. One finding from Figure 3 is that $SPI_{-0.8}$ tends to miss droughts, which according to Figure 5b results from a delayed start of droughts. In contrast, drought appears in RF after SPI_0 over the majority of the state, with the largest difference observed in the wettest part of the state. The reason is likely that SPI does not know how resilient the system is. For example, after several rainy months, water is abundant, and a month of abnormally low rain would not necessarily lead to a drought. While SPI accumulated over longer time periods than 1 month is likely to better capture the resilience of the system since it has longer *P* memory, at 1 month accumulation period the SPI has higher correlation with RF and a smaller drought onset difference (Figure S1 in the Supporting Information S1). It has been reported that SPI computed for a short accumulation period is more suitable for use as a drought indicator for immediate impacts (European Commission, 2020). Figures 5b and 5c suggest that neither of the two drought thresholds is optimal, and a better threshold value is likely to be between 0 and −0.8.

Figure 5e shows that the drought appears in RF with a small lag of ±1 month compared to EDDI. RF shows drought emergence before EDDI in the majority of the state except areas in the west central and the southwest. Considering the low correlation in the wet parts of the state and the low "True negative" score achieved by EDDI in Figure 3, EDDI appears to not capture drought dynamics under drought-breaking flash events such as tropical storms and hurricanes that hit the eastern part of the state.

The RF drought indicator quantifies the probability of drought rather than its categorical severity as in EDDI, SPI, PDSI and USDM. Drought probability represents the conditional probability given the current climate (see Section 2.3.2 for details). Monitoring drought probabilities and how they are evolving in time allows for recognizing a drought before it occurs (probability increases to near 0.5) or intensifies. We argue that drought probabilities provide a more reliable quantification of drought than severity categories, as they are not based on distribution assumptions nor are they computed in reference to a climatology. This is unlike the other drought indicators which assume a fixed number of droughts (percentile) falling in each drought category during a climatological period. Furthermore, the derived drought probabilities take into account the interaction of a range of climate variables in the land-ocean-atmosphere system that can influence droughts.

3.4. Importance of Climate Features in Explaining Droughts

We generated 100 RF models and computed the importance of each predictor variable as the average of its conditional permutation importance across all forests. As described in Section 2.3.2, the importance of a given predictor variable, for example, ET, is the difference in prediction accuracy before and after permuting ET averaged over all permutations. Table 2 shows the mean and the range of importance of each predictor variable across the 100 RF models, and its ranking. All the variables appear to offer useful information to discern "drought" and

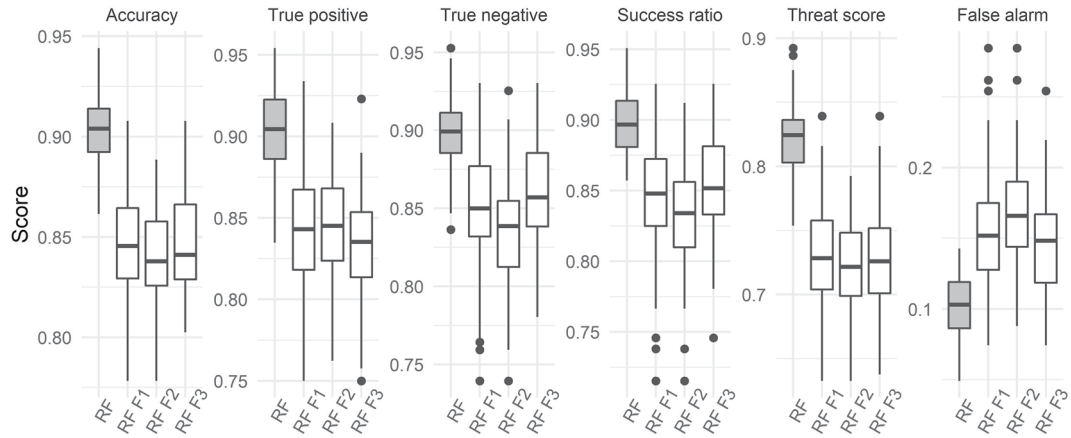

Figure 6. Performance results of RF classifier and RF drought indicators, RF F1, RF F2 and RF F3 at testing samples across 100 different sub-sampling of training and testing samples. Performance scores are explained in Section 2.5.

"no drought", since they all have non-zero importance. Also, as expected, precipitation is the climate feature that provides the maximum information about drought, followed by ENSO and SM. SM_{prev} comes next, its high importance is likely to come from its provision of moisture memory and a signal of system resilience. ET and CWS empower drought predictions equally, followed by PET and NDVI. The month feature was the least important variable.

Despite *P* being more important to drought than PET, PET anomalies can depict the beginning of drought better than *P* anomalies, at least as embodied in EDDI and SPI respectively, as inferred from Figure 5. One example of a situation where relying on *P* anomalies can be misleading is when abnormally low precipitation occurs after several wet months. In this case a drought will appear in the SPI signal, whereas in reality water is abundant and the lack of rain will not necessarily lead to drought emergence. Another example is that abnormally high PET can lead to drought even when precipitation is near normal (Lukas et al., 2017) in which case, drought will not be indicated by SPI.

3.5. RF Forecast Models

In a further analysis, we use RF to build three forecast models—RF F1, RF F2 and RF F3—that quantify drought 1, 2 and 3 months ahead, respectively. In the training process, each event record consists of a label ("drought", "no drought") observed at a month, and climate features observed 1 (RF F1), 2 (RF F2) and 3 (RF F3) months before. We assess the predictive skill of these forecast models following the same out-of-sample testing approach described in Section 2.5. Figure 6 illustrates the results of the out-of-sample performance of RF drought indicator and each forecast model across 100 different testing datasets. The three forecast models score above 83% in "Accuracy", "True positive", "True negative", and "Success ratio" across the majority of the out-of-sample testing, but as expected, could not beat the scores of the RF drought indicator with concurrent predictor variables. These values are comparable or better than EDDI, PDSI or SPI with concurrent predictor variables (Figure 3) and so offer hope for successful short-term predictive capacity.

We also assessed how well the forecast models replicate the probability derived by the RF drought indicators. For this analysis, we calculate four new performance metrics at each of the testing events, and 100 testing datasets to measure the discrepancy of the forecast models with the RF drought indicator. The employed metrics are root mean squared error (RMSE), standard deviation (SD) difference, correlation and mean absolute bias. The results in Figure 7 show that the discrepancy between forecasted drought probabilities and the actual drought probability slightly increases as the forecast period increases as expected.

Finally, Figure 8 shows maps of the correlation of the three forecast models with the RF drought indicator during the drought episode January 2010-April 2012. Similar to our previous findings from Figure 7, correlation decreases as the forecast period increases, particularly in the wet east of the state. The lag in the drought onset

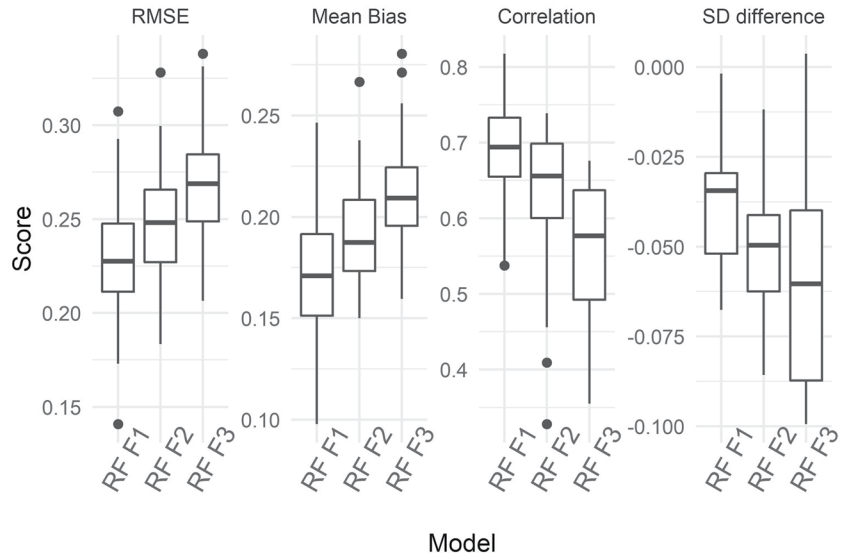

Figure 7. Performance of the three forecast models RF F1, RF F2 and RF F3 relative to RF drought indicator.

is presented in Figures 8d–8f for RF F1, RF F2 and RF F3 respectively. The onset difference maps show that the onset lag is in the range ±1 in the west for all the three forecast models, whereas in the east the forecast models tend to delay drought as the forecast period increases.

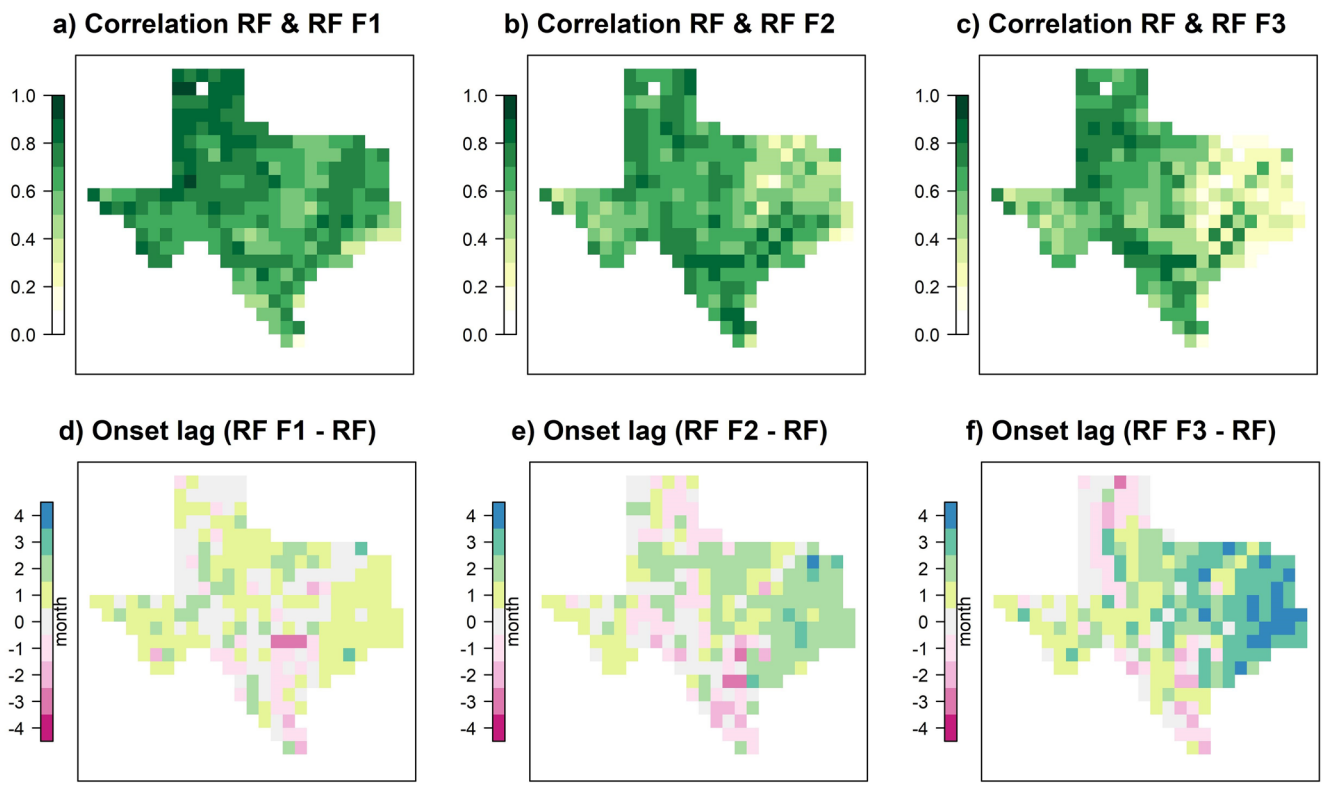

Figure 8. Correlation between RF drought probabilities and (a) RF F1, (b) RF F2, and (c) RF F3. Difference in RF drought onset and each of (d) RF F1, (e) RF F2, and (f) RF F3.

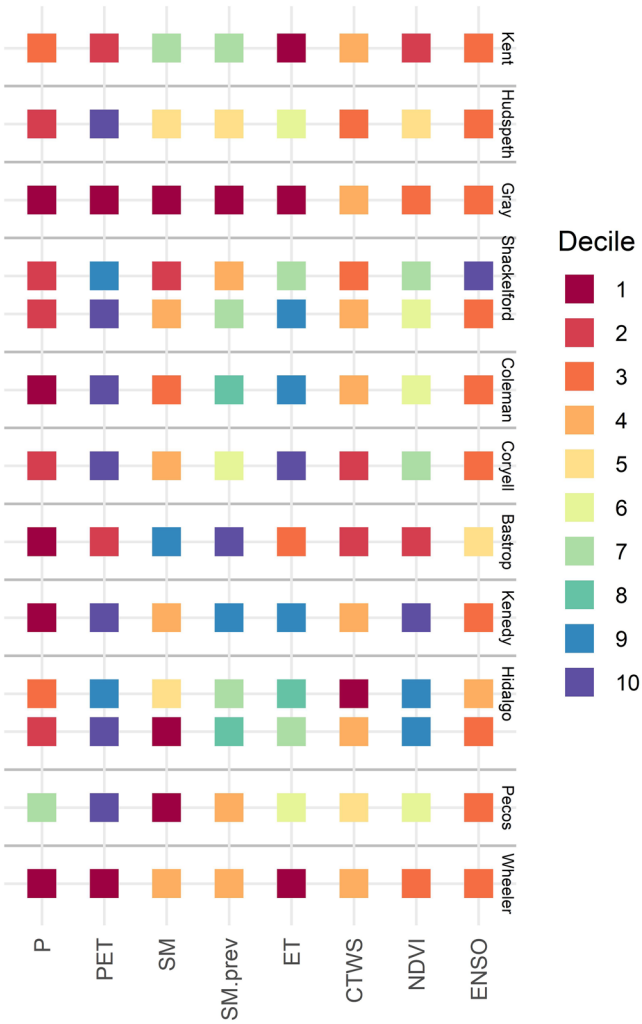

Figure 9. The suite of hydrological circumstances and location (Texan counties) where impactful monthly drought events were not detected by EDDI and SPI. Circumstances are expressed as the deciles of precipitation (*P*), surface soil moisture (SM), PET, actual evapotranspiration (ET), change in water storage (CWS), Normalised Difference Vegetation Index (NDVI), and El Niño-Southern Oscillation (ENSO) that occurred during drought.

4. Discussion

4.1. The New RF Drought Indicator Versus USDM

The advanced capabilities of the RF approach and USDM in discerning "droughts" and "non droughts" compared to EDDI, SPI and PDSI highlight the importance of analyzing the collective changes in climate features to better support drought quantification.

USDM is the current state of the art index of the weekly drought conditions in the U.S.; the new RF drought indicator provides a valuable counterpart to USDM for drought monitoring at the monthly scale. There are however several advantages in using the RF approach: (a) the RF algorithm is developed once, then building drought probability maps from current climate data is an automated process. In comparison, deriving USDM maps is not automated as it incorporates subjective opinion and experts' interpretation; (b) The spatial resolution of the RF drought indicator is 0.5° (or higher where finer resolution inputs are available), whereas USDM provides a big picture of the drought conditions over 10 Texan climate regions. The sparse resolution of USDM did not allow it to resolve droughts at the grid scale and resulted in prediction errors in the out-of-sample tests (Figure 3); (c) USDM provides discrete drought categories, with limited ways for analyzing them, and no clear method on how to aggregate them from weekly to other temporal scales (e.g., monthly). In comparison, the RF algorithm can be trained on data aggregated over several months and then applied to quantify droughts with longer time frames; (d) The RF approach shows good forecast capabilities, while USDM does not have any forecast capabilities. This is true both in terms of the lag models demonstrated here, and the applicability of the RF approach to climate model projection data.

4.2. Circumstances During Droughts Not Detected by SPI and EDDI

The occurrence of drought impact is multifactorial. Drought indices typically identify droughts by tracking the relative departures from normal conditions of water-related climate features (e.g., *P* in SPI, PET in EDDI) or the gap between water supply and demand (e.g., *P* and PET in PDSI). The machine learning drought indicator presented here additionally shows that there are some unexpected circumstances where there are impactful droughts not encompassed by traditional drought metrics. Figure 9 shows a suite of circumstances where drought events have not been identified by either SPI nor EDDI. For instance, despite rain (7th decile *P*) at the beginning of summer 2016, drought in Pecos developed from high atmospheric water demand (10th decile PET) due to elevated temperatures, vegetation started to turn brown (DIR35974, 6th decile NDVI) and soil moisture dropped to its lowest levels. In comparison, drought in Bastrop at the end of winter 2015 was characterized by very low rates of rain (1st decile *P*) and large decline in groundwater (2nd decile CWS). Soil moisture was abundant despite drought as a result of cold weather and the reliance of vegetation, that is, deep-rooted oak trees, on groundwater. In Coleman, drought emerged from the combined effect of high atmospheric water demand (10th decile PET) and low precipitation rates (1st decile). High ET rates (9th decile) led moisture to drop quickly (from 8th decile in the previous month to 3rd decile. These conditions marked the beginning of drought in Coleman in summer 2016. Continuing drought in Wheeler and Gray in winter 1996 was characterized by low rates of *P*, PET and ET, and a decline in groundwater. Droughts in Hidalgo were driven by low *P* rates (third and 2nd decile) and high PET (ninth and 10th decile) in the summer of 1984 (top row) and 2016 (bottom row) respectively. The drought event was characterized with a large decrease in groundwater in 1984 (1st decile CWS). In comparison, during the 2016 drought, soil moisture declined significantly (from decile eighth to 1st decile). SPI and EDDI which track anomalies in *P* and PET respectively, were not able to identify any of these drought events. By focusing on

the actual drought events, machine learning can identify all the combinations of conditions that lead to drought, as evidenced by observations, rather than relying on a priori intuition.

4.3. Transferability of the RF Approach to New Regions

The range of factors that affect the onset and development of droughts are a mixture of large-scale factors that are shared among different regions over land (such as a lack of precipitation) and unique local scale factors such as vegetation properties, land cover, water-related activities, and water resources management. Machine learning allows us to incorporate both large- and local-scale information to identify droughts.

The new RF drought indicator was developed by training a RF algorithm on patterns within the Texan region. Therefore, the particular RF drought indicator derived here is specific to Texas and should not be used to monitor and quantify droughts in new locations outside Texas. Clearly the physical processes linked with the initiation and persistence of drought are different over different regions around the world. One obvious example is that droughts in Texas are related to the cold phase of ENSO, whereas in many regions on land, droughts are related to the warm phase of ENSO (i.e., El Niño, e.g., Australia). However, the approach is entirely portable, assuming new RF models are developed for new locations and historical drought data of sufficient quantity and reliability exist in those locations. For example, in Europe, reports on historical drought events are available from The European Drought Reference database and the European Drought Impact Report Inventory and accessed through https://www.geo.uio.no/edc/droughtdb/. In Australia, monthly climate reports describing the wet and dry conditions across the state are produced by the Australian Bureau of Meteorology and are made publicly available at http://www.bom.gov.au/climate/current/statement_archives.shtml.

4.4. Future Research Directions

There are a number of key processes linked with the initiation and persistence of drought that could be incorporated to improve the predictive skills of the RF drought indicator but were not included here, for example, zonal moisture advection (Erfanian & Fu, 2019). Nevertheless, as new relevant climate variables become available, it is easy to test their ability to improve predictions, and if justified, incorporate them as additional predictors.

We used a RF to generate spatial predictions of drought. However, the spatial location of points was ignored in the modeling process, so that spatial autocorrelation was not accounted for. Hengl et al. (2018) developed a new framework called Random Forest for spatial data (RFsp) that extends RF to account for spatial dependence. The RFsp framework incorporates distances from observation points as predictor variables and therefore, adds geographical proximity effects into the prediction process. More recently (Georganos et al., 2019), developed a novel geographical implementation of RF, named Geographical Random Forest (GRF) that addresses spatial heterogeneity by disaggregating RF into geographical space in the form of local sub-models. GRF is implemented in the R package SpatialML (http://lctools.science/). We anticipate that applying any of the RFsp or the GRF approach in the future will further improve the performance of the RF drought indicators and the predictive skills of the RF forecasting models. It is important to note that both approaches require a larger number of grid cells than what was used here.

Another topic for future research is using deep learning as an alternative, and more powerful approach than RF to capture the spatio-temporal characteristics of droughts (Reichstein et al., 2019). A few studies implemented deep learning for drought quantification (e.g., Deo & Şahin, 2015; Shen et al., 2019). These studies used drought indicators as spatially and temporally continuous labels. However, this approach is not optimal as drought indicators suffer from biases and should not be used as "ground-truth" labels. Given the absence of spatially and temporally continuous drought data, using deep learning to quantify droughts remains challenging.

5. Conclusions

In contrast to most scientific drought metrics, in this work we used recorded drought impacts as our observational definition of drought, and used a RF model to establish an empirical relationship between drought impact and a broad range of drought-related climate predictors. The derived RF drought indicator performed as well out-of-sample as the assimilated drought product USDM. However, unlike USDM, the approach offers considerable predictive ability, both in the short-term drought predictions and use with climate projections. Also, this approach

was able to predict unseen drought impact events with far greater success than existing climate-variable based drought metrics, such as SPI, PDSI or EDDI. While these drought metrics often give us a clear indication of drought impacts, drought impact is multifactorial. The presented approach allows us to utilize drought impact data to understand the full suite of circumstances that lead to impactful droughts. While Texas was used as a test case here, the approach is applicable to any region with sufficient spatiotemporal drought records.

Data Availability Statement

Data used in this is available through these papers (Dorigo et al., 2017; Gruber et al., 2017, 2019; Harris et al., 2014; Hobeichi et al., 2021; Humphrey & Gudmundsson, 2019; Liu et al., 2012; Pinzon & Tucker, 2014; Schneider et al., 2018; Smith & Sardeshmukh, 2000) or described in Wilhite et al. (2007). We thank all the data owners for making their data publicly available.

Acknowledgments
The authors acknowledge the support of the Australian Research Council Centre of Excellence for Climate Extremes (CE170100023). A.M.U. acknowledges support from the ARC Discovery Early Career Researcher Award (DE200100086). This research was undertaken with the assistance of resources and services from the National Computational Infrastructure (NCI), which is supported by the Australian Government.

References

AMS. (1997). Policy statement. *Society, Bulletin of the American Meteorological*, *78*(5), 847–852. https://doi.org/10.1175/1520-0477-78.5.847

AWG. (2004). *Creating a drought early warning system for the 21st century: The national integrated drought information system. Western Governors Report*. Denver, CO: Western Governors Association.

Azmi, M., Ruediger, C., & Walker, J. P. (2016). A data fusion-based drought index. *Water Resources Research*, *52*, 2222–2239. https://doi.org/10.1002/2015WR017834

Bachmair, S., Kohn, I., & Stahl, K. (2015). Exploring the link between drought indicators and impacts. *Natural Hazards and Earth System Sciences*, *15*(6), 1381–1397. https://doi.org/10.5194/nhess-15-1381-2015

Balakrishnama, S., & Ganapathiraju, A. (1998). Linear discriminant analysis—A brief tutorial. *Institute for Signal and Information Processing*, *18*(1998), 1–8.

Beguería, S., Vicente-Serrano, S. M., Reig, F., & Latorre, B. (2014). Standardized precipitation evapotranspiration index (SPEI) revisited: Parameter fitting, evapotranspiration models, tools, datasets and drought monitoring. *International Journal of Climatology*, *34*(10), 3001–3023.

Breiman, L. (2001). Random forests. *Machine Learning*, *45*(1), 5–32. https://doi.org/10.1023/A:1010933404324

Breiman, L., Friedman, J., Stone, C. J., & Olshen, R. A. (1984). *Classification and regression trees*. CRC Press.

Brown, J. F., Wardlow, B. D., Tadesse, T., Hayes, M. J., & Reed, B. C. (2008). The vegetation drought response index (VegDRI): A new integrated approach for monitoring drought stress in vegetation. *GIScience and Remote Sensing*, *45*(1), 16–46. https://doi.org/10.2747/1548-1603.45.1.16

Combs, S. (2014). Going deeper for the solution. *Texas Water Report*.

Cutler, D. R., Edwards, T. C., Jr, Beard, K. H., Cutler, A., Hess, K. T., Gibson, J., & Lawler, J. J. (2007). Random forests for classification in ecology. *Ecology*, *88*(11), 2783–2792.

Dai, A., & National Center for Atmospheric Research Staff (Eds). (2019). The Climate Data Guide: Palmer Drought Severity Index (PDSI). Retrieved from https://climatedataguide.ucar.edu/climate-data/palmer-drought-severity-index-pdsi

Davis, T. W., Prentice, I. C., Stocker, B. D., Thomas, R. T., Whitley, R. J., Wang, H., et al. (2017). Simple process-led algorithms for simulating habitats (SPLASH v. 1.0): Robust indices of radiation, evapotranspiration and plant-available moisture. *Geoscientific Model Development*, *10*(2), 689–708.

Deo, R. C., & Şahin, M. (2015). Application of the extreme learning machine algorithm for the prediction of monthly Effective Drought Index in eastern Australia. *Atmospheric Research*, *153*, 512–525. https://doi.org/10.1016/j.atmosres.2014.10.016

Dorigo, W., Wagner, W., Albergel, C., Albrecht, F., Balsamo, G., Brocca, L., et al. (2017). ESA CCI Soil Moisture for improved Earth system understanding: State-of-the art and future directions. *Remote Sensing of Environment*, *203*, 185–215.

Erfanian, A., & Fu, R. (2019). The role of spring dry zonal advection in summer drought onset over the US Great Plains. *Atmospheric Chemistry and Physics*, *19*(24).

European Commission. (2020). *EDO indicator factsheet: Standardized Precipitation Index (SPI)*. Retrieved from https://edo.jrc.ec.europa.eu/

Fernández-Delgado, M., Cernadas, E., Barro, S., & Amorim, D. (2014). Do we need hundreds of classifiers to solve real world classification problems? *Journal of Machine Learning Research*, *15*, 3133–3181. https://doi.org/10.1117/1.JRS.11.015020

Fernando, D. N., Chakraborty, S., Fu, R., & Mace, R. E. (2019). A process-based statistical seasonal prediction of May-July rainfall anomalies over Texas and the Southern Great Plains of the United States. *Climate Services*, 100133. https://doi.org/10.1016/j.cliser.2019.100133

Folger, P. F., Cody, B. A., & Carter, N. T. (2012). *Drought in the United States: Causes and issues for congress*. Congressional Research Service.

Friedman, J. H. (1991). Multivariate adaptive regression splines. *Annals of Statistics*, 1–67.

Georganos, S., Grippa, T., Niang Gadiaga, A., Linard, C., Lennert, M., Vanhuysse, S., et al. (2019). Geographical random forests: A spatial extension of the random forest algorithm to address spatial heterogeneity in remote sensing and population modelling. *Geocarto International*, *36*(2), 121–136. https://doi.org/10.1080/10106049.2019.1595177

Grigg, N. S. (2014). The 2011–2012 drought in the United States: New lessons from a record event. *International Journal of Water Resources Development*, *30*(2), 183–199.

Gruber, A., Dorigo, W. A., Crow, W., & Wagner, W. (2017). Triple collocation-based merging of satellite soil moisture retrievals. *IEEE Transactions on Geoscience and Remote Sensing*, *55*(12), 6780–6792.

Gruber, A., Scanlon, T., van der Schalie, R., Wagner, W., & Dorigo, W. (2019). Evolution of the ESA CCI Soil Moisture climate data records and their underlying merging methodology. *Earth System Science Data*, *11*(2), 717–739.

Hao, Z., Singh, V. P., & Xia, Y. (2018). Seasonal drought prediction: Advances, challenges, and future prospects. *Reviews of Geophysics*, *56*(1), 108–141. https://doi.org/10.1002/2016RG000549

Harris, I., Jones, P. D., Osborn, T. J., & Lister, D. H. (2014). Updated high-resolution grids of monthly climatic observations—The CRU TS3.10 Dataset. *International Journal of Climatology*, *34*(3), 623–642. https://doi.org/10.1002/joc.3711

Heim, R. R., Jr. (2002). A review of twentieth-century drought indices used in the United States. *Bulletin of the American Meteorological Society*, *83*(8), 1149–1166.

Hengl, T., Nussbaum, M., Wright, M. N., Heuvelink, G. B. M., & Gräler, B. (2018). Random forest as a generic framework for predictive modeling of spatial and spatio-temporal variables. *PeerJ*, *2018*(8). https://doi.org/10.7717/peerj.5518

Hobbins, M. T., Wood, A., McEvoy, D. J., Huntington, J. L., Morton, C., Anderson, M., & Hain, C. (2016). The Evaporative Demand Drought Index. Part I: Linking drought evolution to variations in evaporative demand. *Journal of Hydrometeorology*, *17*(6), 1745–1761. https://doi.org/10.1175/JHM-D-15-0121.1

Hobeichi, S. (2020). *Derived optimal linear combination evapotranspiration—DOLCE v2.1*. CLEX. https://doi.org/10.25914/5f1664837ef06

Hobeichi, S., Abramowitz, G., & Evans, J. P. (2021). Robust historical evapotranspiration trends across climate regimes. *Hydrology and Earth System Sciences*, *25*, 3855–3874. https://doi.org/10.5194/hess-25-3855-2021

Hughes, N., Ying, W., Boult, C., & Lawson, K. (2020). Defining drought from the perspective of Australian farmers—Department of Agriculture. Australian GovernmentlABARES, Working paper (November) (pp. 1–29). https://doi.org/10.25814/fngh-wm22

Humphrey, V., & Gudmundsson, L. (2019). GRACE-REC: A reconstruction of climate-driven water storage changes over the last century. *Earth System Science Data*, *11*(3), 1153–1170.

IPCC. (2014). Climate Change 2014: Synthesis Report. Contribution of Working Groups I, II and III to the Fifth Assessment Report of the Intergovernmental Panel on Climate Change [Core Writing Team, R.K. Pachauri and L.A. Meyer (eds.)].

Karnieli, A., Agam, N., Pinker, R. T., Anderson, M., Imhoff, M. L., Gutman, G. G., et al. (2010). Use of NDVI and land surface temperature for drought assessment: Merits and limitations. *Journal of Climate*, *23*(3), 618–633.

Keyantash, J., & Dracup, J. A. (2002). The quantification of drought: An evaluation of drought indices. *Bulletin of the American Meteorological Society*, *83*, 1167–1180.

Keyantash, J. A., & Dracup, J. A. (2004). An aggregate drought index: Assessing drought severity based on fluctuations in the hydrologic cycle and surface water storage. *Water Resources Research*, *40*(9).

Khan, N., Sachindra, D. A., Shahid, S., Ahmed, K., Shiru, M. S., & Nawaz, N. (2020). Prediction of droughts over Pakistan using machine learning algorithms. *Advances in Water Resources*, *139*, 103562. https://doi.org/10.1016/j.advwatres.2020.103562

Kruppa, J., Liu, Y., Diener, H., Holste, T., Weimar, C., König, I. R., & Ziegler, A. (2014). Probability estimation with machine learning methods for dichotomous and multicategory outcome: Applications. *Biometrical Journal*, *56*(4), 564–583.

Kuhn, M. (2008). Building predictive models in R using the caret package. *Journal of Statistical Software*, *28*(5), 1–26.

Li, Q., Li, P., Li, H., & Yu, M. (2015). Drought assessment using a multivariate drought index in the Luanhe River basin of Northern China. *Stochastic Environmental Research and Risk Assessment*, *29*(6), 1509–1520.

Liaw, A., & Wiener, M. (2002). Classification and regression by randomForest. *R News*, *2*(3), 18–22.

Liu, Y. Y., Dorigo, W. A., Parinussa, R. M., de Jeu, R. A. M., Wagner, W., McCabe, M. F., et al. (2012). Trend-preserving blending of passive and active microwave soil moisture retrievals. *Remote Sensing of Environment*, *123*, 280–297. https://doi.org/10.1016/j.rse.2012.03.014

Lukas, J., Hobbins, M., & Rangwala, I. (2017). *The EDDI user guide v1.0*. Retrieved from https://www.esrl.noaa.gov/psd/eddi/pdf/EDDI_UserGuide_v1.0.pdf

Malley, J. D., Kruppa, J., Dasgupta, A., Malley, K. G., & Ziegler, A. (2012). Probability machines: Consistent probability estimation using nonparametric learning machines. *Methods of Information in Medicine*, *51*(1), 74–81. https://doi.org/10.3414/ME00-01-0052

McGovern, A., Elmore, K. L., Gagne, D. J., Haupt, S. E., Karstens, C. D., Lagerquist, R., et al. (2017). Using artificial intelligence to improve real-time decision-making for high-impact weather. *Bulletin of the American Meteorological Society*, *98*(10), 2073–2090.

McKee, T. B. (1995). *Drought monitoring with multiple time scales*. Proceedings of 9th Conference on Applied Climatology, Boston.

McKee, T. B., Doesken, N. J., & Kleist, J. (1993). *The relationship of drought frequency and duration to time scales*. Proceedings of the 8th Conference on applied Climatology, Boston (Vol. *17*, pp. 179–183).

Mitchell, T. M. (1997). Does machine learning really work? *AI Magazine*, *18*(3), 11.

Nanzad, L., Zhang, J., Tuvdendorj, B., & Nabil, M. (2019). NDVI anomaly for drought monitoring and its correlation with climate factors over Mongolia from 2000 to 2016. *Journal of Arid Environments*, *164*, 69–77. https://doi.org/10.1016/j.jaridenv.2019.01.019

Nelder, J. A., & Wedderburn, R. W. M. (1972). Generalized linear models. *Journal of the Royal Statistical Society: Series A*, *135*(3), 370–384.

Palmer, W. C. (1965). *Meteorological drought* (Vol. 45, p. 58). Office of Climatology, US Department of Commerce.

Park, S., Im, J., Jang, E., & Rhee, J. (2016). Drought assessment and monitoring through blending of multi-sensor indices using machine learning approaches for different climate regions. *Agricultural and Forest Meteorology*, *216*, 157–169.

Pinzon, J. E., & Tucker, C. J. (2014). A non-stationary 1981–2012 AVHRR NDVI3g time series. *Remote Sensing*, *6*(8), 6929–6960.

Pu, B., Fu, R., Dickinson, R. E., & Fernando, D. N. (2016). Why do summer droughts in the Southern Great Plains occur in some La Niña years but not others? *Journal of Geophysical Reseach: Atmospheres*, *121*, 1120–1137. https://doi.org/10.1002/2015JD023508

Reichstein, M., Camps-Valls, G., Stevens, B., Jung, M., Denzler, J., Carvalhais, N., & Prabhat (2019). Deep learning and process understanding for data-driven Earth system science. *Nature*, *566*(7743), 195–204. https://doi.org/10.1038/s41586-019-0912-1

Rodriguez-Galiano, V. F., Ghimire, B., Rogan, J., Chica-Olmo, M., & Rigol-Sanchez, J. P. (2012). An assessment of the effectiveness of a random forest classifier for land-cover classification. *ISPRS Journal of Photogrammetry and Remote Sensing*, *67*, 93–104.

Sandri, M., & Zuccolotto, P. (2008). A bias correction algorithm for the gini variable importance measure in classification trees. *Journal of Computational & Graphical Statistics*, *17*(3), 611–628. https://doi.org/10.1198/106186008X344522

Schneider, U., Becker, A., Finger, P., Meyer-Christoffer, A., & Ziese, M. (2018). GPCC full data monthly product version 2018 at 0.5°: Monthly land-surface precipitation from rain-gauges built on GTS-based and historical data. Global Precipitation Climatology Centre. Retrieved from https://psl.noaa.gov/data/gridded/data.gpcc.html

Scholkopf, B., Sung, K.-K., Burges, C. J. C., Girosi, F., Niyogi, P., Poggio, T., & Vapnik, V. (1997). Comparing support vector machines with Gaussian kernels to radial basis function classifiers. *IEEE Transactions on Signal Processing*, *45*(11), 2758–2765.

Schubert, S. D., Suarez, M. J., Pegion, P. J., Koster, R. D., & Bacmeister, J. T. (2004). Causes of long-term drought in the US Great plains. *Journal of Climate*, *17*(3), 485–503.

Seager, R., Goddard, L., Nakamura, J., Henderson, N., & Lee, D. E. (2014). Dynamical causes of the 2010/11 Texas-northern Mexico drought. *Journal of Hydrometeorology*, *15*(1), 39–68. https://doi.org/10.1175/JHM-D-13-024.1

Seneviratne, S. I., Nicholls, N., Easterling, D., Goodess, C. M., Kanae, S., Kossin, J., et al. (2012). Changes in climate extremes and their impacts on the natural physical environment. In C. B. Field, V. Barros, T. F. Stocker, D. Qin, D. J. Dokken, K. L. Ebi, et al. (Eds.), *Managing the risks of extreme events and disasters to advance climate change adaptation* (pp. 109–230). A Special Report of Working Groups I and II of the Intergovernmental Panel on Climate Change (IPCC). Cambridge University Press.

Shen, R., Huang, A., Li, B., & Guo, J. (2019). Construction of a drought monitoring model using deep learning based on multi-source remote sensing data. *International Journal of Applied Earth Observation and Geoinformation*. https://doi.org/10.1016/j.jag.2019.03.006

Smith, C. A., & Sardeshmukh, P. D. (2000). The effect of ENSO on the intraseasonal variance of surface temperatures in winter. *International Journal of Climatology: A Journal of the Royal Meteorological Society*, *20*(13), 1543–1557.

Soh, Y. W., Koo, C. H., Huang, Y. F., & Fung, K. F. (2018). Application of artificial intelligence models for the prediction of standardized precipitation evapotranspiration index (SPEI) at Langat River Basin, Malaysia. *Computers and Electronics in Agriculture*, *144*, 164–173. https://doi.org/10.1016/j.compag.2017.12.002

Stagge, J. H., Tallaksen, L. M., Gudmundsson, L., Van Loon, A. F., & Stahl, K. (2015). Candidate distributions for climatological drought indices (SPI and SPEI). *International Journal of Climatology*, *35*(13), 4027–4040.

Strobl, C., Boulesteix, A.-L., Kneib, T., Augustin, T., & Zeileis, A. (2008). Conditional variable importance for random forests. *BMC Bioinformatics*, *9*(1), 307. https://doi.org/10.1186/1471-2105-9-307

Strobl, C., Boulesteix, A. L., Zeileis, A., & Hothorn, T. (2007). Bias in random forest variable importance measures: Illustrations, sources and a solution. *BMC Bioinformatics*, *8*. https://doi.org/10.1186/1471-2105-8-25

Svoboda, M., LeComte, D., Hayes, M., Heim, R., Gleason, K., Angel, J., et al. (2002). The drought monitor. *Bulletin of the American Meteorological Society*, *83*(8), 1181–1190.

Swain, P. H., & Hauska, H. (1977). The decision tree classifier: Design and potential. *IEEE Transactions on Geoscience Electronics*, *15*(3), 142–147.

Texas Water Development Board. (2012). Chapter 4 climate of Texas. Water for Texas 2012 State Water Plan (pp. 145–155). Retrieved from https://www.mendeley.com/viewer/?fileId=0ec0c4ff-06ba-832f-0042-1a4fa3e46231&documentId=0abfb413-0a9d-3fa4-8c83-87957a3263c7

Ukkola, A. M., Pitman, A. J., De Kauwe, M. G., Abramowitz, G., Herger, N., Evans, J. P., & Decker, M. (2018). Evaluating CMIP5 model agreement for multiple drought metrics. *Journal of Hydrometeorology*, *19*(6), 969–988. https://doi.org/10.1175/jhm-d-17-0099.1

Van Loon, A. F., & Van Lanen, H. A. J. (2012). A process-based typology of hydrological drought. *Hydrology and Earth System Sciences*, *16*(7), 1915–1946.

Walter, I. A., Allen, R. G., Elliott, R., Jensen, M. E., Itenfisu, D., Mecham, B., et al. (2000). ASCE's standardized reference evapotranspiration equation. In *Watershed management and operations management* (Vol. 2000, pp. 1–11).

Wilhite, D. A. (2009). Drought monitoring as a component of drought preparedness planning. In *Coping with drought risk in agriculture and water supply systems* (pp. 3–19). Springer.

Wilhite, D. A., & Glantz, M. H. (1985). Understanding: The drought phenomenon: The role of definitions. *Water International*, *10*(3), 111–120. https://doi.org/10.1080/02508068508686328

Wilhite, D. A., Svoboda, M. D., & Hayes, M. J. (2007). Understanding the complex impacts of drought: A key to enhancing drought mitigation and preparedness. *Water Resources Management*, *21*(5), 763–774. https://doi.org/10.1007/s11269-006-9076-5

Wright, M. N., & Ziegler, A. (2017). ranger: A fast implementation of random forests for high dimensional data in C++ and R. *Journal of Statistical Software*, *77*, 1–17. https://doi.org/10.18637/jss.v077.i01

Xu, L., Abbaszadeh, P., Moradkhani, H., Chen, N., & Zhang, X. (2020). Continental drought monitoring using satellite soil moisture, data assimilation and an integrated drought index. *Remote Sensing of Environment*, *250*, 112028. https://doi.org/10.1016/j.rse.2020.112028

Xu, L., Chen, N., & Zhang, X. (2018). A comparison of large-scale climate signals and the North American Multi-Model Ensemble (NMME) for drought prediction in China. *Journal of Hydrology*, *557*, 378–390. https://doi.org/10.1016/j.jhydrol.2017.12.044

Xu, L., Chen, N., & Zhang, X. (2019). Global drought trends under 1.5 and 2°C warming. *International Journal of Climatology*, *39*(4), 2375–2385. https://doi.org/10.1002/joc.5958

Yang, Z., Zhang, Q., Hao, X., & Yue, P. (2019). Changes in evapotranspiration over global semiarid regions 1984–2013. *Journal of Geophysical Research: Atmospheres*, *124*(6), 2946–2963. https://doi.org/10.1029/2018JD029533

Yihdego, Y., Vaheddoost, B., & Al-weshah, R. A. (2019). Drought indices and indicators revisited. *Arabian Journal of Geosciences*, *12*(69), 1–12. https://doi.org/10.1007/s12517-019-4237-z

Zhang, A., & Jia, G. (2013). Monitoring meteorological drought in semiarid regions using multi-sensor microwave remote sensing data. *Remote Sensing of Environment*, *134*, 12–23.

Zou, H., & Hastie, T. (2005). Regularization and variable selection via the elastic net. *Journal of the Royal Statistical Society: Series B*, *67*(2), 301–320.